Collisional redistribution in Sr–He spinchanging energy transfer collisions: Finalstate alignment

Sharath Ananthamurthy and P. D. Kleiber

Citation: The Journal of Chemical Physics **102**, 1917 (1995); doi: 10.1063/1.468757
View online: http://dx.doi.org/10.1063/1.468757
View Table of Contents: http://scitation.aip.org/content/aip/journal/jcp/102/5?ver=pdfcov
Published by the AIP Publishing

Collisional redistribution in Sr–He spin-changing energy transfer collisions: Final-state alignment

Sharath Ananthamurthy[a] and P. D. Kleiber
Department of Physics and Astronomy, University of Iowa, Iowa City, Iowa 52242

(Received 2 September 1994; accepted 27 October 1994)

We have measured the product alignment resulting from the collisional redistribution of polarized light in Sr–He inelastic spin-changing energy transfer collisions. The experimental results are in good agreement with the predictions of an analytic theoretical model, based on a standard orbital-locking and following approximation, but generalized to this inelastic collision process. The good agreement indicates a clear understanding of the energy transfer dynamics in this case, and suggests that this simple analytic approach may be generalized to a much broader range of collisional phenomena. © *1995 American Institute of Physics.*

I. INTRODUCTION

One experimental approach to the study of orbital alignment effects on collision dynamics involves the use of far wing laser scattering techniques.[1–4] In the far or quasistatic wing of a collision-broadened atomic spectral line, the Franck–Condon approximation describes an absorption event as occurring at a fixed internuclear separation between well-defined adiabatic Born–Oppenheimer states of the transient collision complex.[4] This makes it possible to selectively excite states of well-characterized electronic symmetry, corresponding to states of specific reagent electronic orbital alignment in the collision complex.[4] The total absorption profiles in such experiments are determined largely by the shape of the intermolecular potential energy curves. Final state resolved measurements of the far wing action spectra are sensitive to the dynamical evolution through the excited state ''half-collision'' from the Condon point of excitation into the asymptotic distribution of product states, giving insight into the nonadiabatic couplings in the exit channel.

In earlier work we applied these techniques to a study of CaHe collisional energy transfer.[1,2] In these experiments, a laser was tuned into the collision-broadened wings of the $Ca(4s^2\ ^1S-5p\ ^1P)$ transition, directly exciting the CaHe ''quasimolecule.''[1,2] This excited, unstable CaHe molecule either evolves through the collision into the $Ca^*(5p\ ^1P)$ level or ''predissociates'' via the spin–orbit curve crossing to the $Ca^*(5p\ ^3P)$ manifold. Based on model potential energy curves, we qualitatively expect that absorption in the far red wing should predominantly excite the attractive $CaHe(5p\ ^1\Pi)$ state, while blue wing absorption probably corresponds to excitation of the repulsive $CaHe(5p\ ^1\Sigma^+)$ curve. Thus these far wing laser absorption techniques may be used to carry out orbitally aligned studies of the collision dynamics under gas cell conditions. Specifically, we have measured both the total far wing absorption and the triplet/singlet branching profile as a function of laser detuning in the wings of the $Ca(4s^2\ ^1S_0 \rightarrow 5p\ ^1P_1)$ resonance transition.[1,2] We have observed a pronounced red wing/blue wing asymmetry in the branching profile[1,2] which strongly supports the conclusions originally drawn by Leone and co-workers[5] that the energy transfer results from a spin–orbit curve crossing between the attractive $5p\ ^1\Pi$ and the repulsive $5p\ ^3\Sigma^+$ states of the CaHe molecule.

Theoretical modeling of these final state resolved laser scattering experiments requires a nonadiabatic theory of collisional line broadening.[2,4,6,7] In the CaHe case this modeling has been carried out by Pouilly using quantum close-coupling methods,[7] and excellent agreement with the experimental line profiles was obtained. We have recently applied a semiclassical (classical path quantum close coupling) nonadiabatic theory of collisional redistribution to model Ca–He spin-changing energy transfer collisions.[2] The theory predicts the total far wing absorption and final state resolved action spectra. The semiclassical model predictions are in excellent agreement with Pouilly's quantum mechanical close-coupling calculations and both are in good accord with the experimental observations.[1,2,7]

More recently we carried out similar experiments and calculations in the analogous SrHe collision system,[3]

$$\mathrm{Sr}(5s^2\ ^1S)+\mathrm{He}+h\omega \rightarrow (\mathrm{SrHe}(5s^2\ ^1\Sigma^+)) \rightarrow (\mathrm{SrHe}(5s\ 6p\ ^1\Pi \text{ or } ^1\Sigma^+))^* \tag{1}$$

followed by

$$(\mathrm{SrHe}(5s\ 6p\ ^1\Pi \text{ or } ^1\Sigma^+))^* \rightarrow \mathrm{Sr}^*(6p\ ^1P)+\mathrm{He}+\Delta E \tag{1a}$$

or

$$\rightarrow \mathrm{Sr}^*(6p\ ^3P, 5p'\ ^3F, 5p'\ ^1D)+\mathrm{He}+\Delta E. \tag{1b}$$

In this case, many more product states are accessible. Also the spin–orbit splitting is larger so that the individual ^3P_j fine-structure states can be resolved in fluorescence, allowing a more definitive test of the theory. The dominant branching is into the $^3P_2$ level.[3,8] The experimental $^3P_2/^1P_1$ branching ratio is qualitatively similar to that observed for the CaHe case and is given in Ref. 3. The classical trajectory close-coupling method again works well (for a reasonable set of model potential curves and choice of spin–orbit coupling parameters), correctly predicting the action spectra for the individual fine-structure states.[3]

[a]Present address: Solid State and Structural Chemistry Unit, Indian Institute of Science, Bangalore, India.

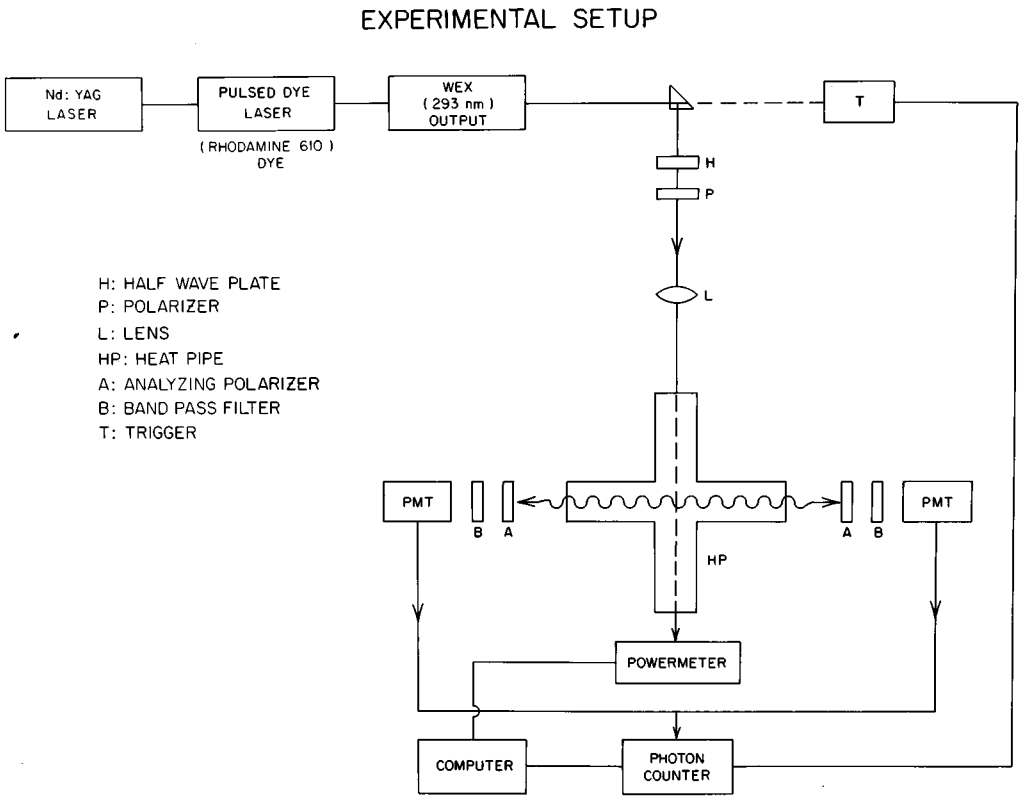

FIG. 1. Experimental arrangement.

Here, we report on the extension of these experimental techniques to include measurements of the final state electronic orbital alignment through observation of the product fluorescence polarization. The results allow more detailed insight into the collisional dynamics, and a much more rigorous test of the semiclassical dynamical model than measurement of population transfer alone. Specifically, we report on studies of the $\mathrm{Sr}(6p\ ^1P_1-4d\ ^1D_2)$ and $\mathrm{Sr}(6p\ ^3P_2-4d\ ^3D_2)$ fluorescence polarization following excitation of the SrHe collision complex in the far wing of the $\mathrm{Sr}(5s^2\ ^1S_0-5s\ 6p\ ^1P_1)$ second resonance transition.

Previously, Cooper, Burnett, and co-workers studied the collisional redistribution of polarized light in quasielastic Sr and Ba–rare gas collisions [analogous to process (1a) above].[9] The experimental fluorescence polarization results were modeled using an "orbital-locking and following" approach[10–12] by Lewis *et al.*[10] This model gives an intuitively appealing picture of the process in terms of the rotation of the molecular electronic orbital through the collision. More detailed quantum close-coupling calculations have also been presented by Julienne.[6] Subsequently, Havey and co-workers,[13] and Behemburg and co-workers[14] applied these experimental techniques to the case of alkali–rare gas fine structure changing collisions. Havey has shown that the orbital-locking and following approach can be extended to include the effects of spin–orbit coupling.[13]

Here we generalize this semiclassical orbital-locking and following method to explain the final state alignment in the collisional redistribution of polarized light in inelastic spin-changing energy transfer collisions. Reasonable agreement with our experimental results demonstrate a clear understanding of the dynamics, and suggests that this theoretical approach can be extended to a broad range of much more complicated physical processes.

II. EXPERIMENTAL ARRANGEMENT

Figure 1 shows the experimental setup which is similar to that described in Ref. 1. A pulsed 30 Hz Nd:YAG pumped dye laser is operated with rhodamine 610 dye. The output is frequency doubled in an angle tuned KD*P crystal to the wavelength regions near the $\mathrm{Sr}(5s^2\ ^1S_0\rightarrow 5s\ 6p\ ^1P_1)$ transition at 293 nm. The laser beam has a spectral bandwidth of $\sim 0.25\ \mathrm{cm}^{-1}$, and the near uv output pulse energy is typically 0.35 mJ in a 6 ns pulse. The laser beam is linearly polarized with a Glan–Thomson prism polarizer and focused with a 50 cm fused silica lens to the center of a five-arm stainless steel, resistively heated oven containing strontium and helium. The beam diameter at the oven center is $\sim 500\ \mu\mathrm{m}$ for a typical peak laser intensity of $1.8\times 10^5\ \mathrm{W/cm}^2$. The helium gas also serves as a buffer preventing diffusion and condensation of the hot strontium vapor on the cold oven windows. The oven allows fluorescence observation at right angles to the incoming laser beam in a standard mutually orthogonal excitation-

detection geometry. Temperature measurement is made with a stainless-steel encased chromel-alumel thermocouple in contact with the vapor at the oven center.

At typical operating temperatures, $T \simeq 670$ °C, the strontium density was estimated to be $[\mathrm{Sr}] \sim 10^{15}/\mathrm{cm}^3$ from vapor pressure curve data. This is certainly an upper limit, however, since previous studies in ovens of this type have generally demonstrated a vapor pressure roughly an order of magnitude lower than predicted by vapor pressure curves. A more accurate measurement of the Sr vapor density at this temperature is made by observing the near resonant Rayleigh scattering from Sr.[15] Using this technique we obtain the value $[\mathrm{Sr}] \sim 1 \times 10^{14}/\mathrm{cm}^3$.

The collisionally redistributed fluorescence was collected with an $(f/8)$ imaging system and focused through analyzing polarizers and narrow bandpass filters onto a thermoelectrically cooled photomultiplier tube. The fluorescence signals were amplified with fast preamplifiers (gain×25), and detected with a gated photon counting system. The instrumental gate width was set to 100 ns and averages were taken over 300 pulses.

We monitored either the singlet atomic fluorescence on the $\mathrm{Sr}(6p\ ^1P_1 - 4d\ ^1D_2)$ line at 716.7 nm, or the triplet fluorescence on the $\mathrm{Sr}(6p\ ^3P_2 - 4d\ ^3D_2)$ transition at 634.6 nm. These fluorescence signals were measured as a function of laser detuning from the $\mathrm{Sr}(6p\ ^1P_1)$ resonance in the range $(|\Delta| = |\omega - \omega_0| = 10\text{–}100\ \mathrm{cm}^{-1})$, and as a function of He buffer gas pressure in the range (0.1–300 Torr). Polarization measurements were typically made in the low-pressure range (0.1–10 Torr). The signals were verified to be linear in laser power. For small laser detunings (near line center), neutral density filters were used to decrease the laser power in order to eliminate stimulated emission processes and maintain linearity. The linear polarization, $P = (I_\parallel - I_\perp)/(I_\parallel + I_\perp)$ was then determined for each laser detuning and pressure.

There are a number of ways in which the nascent alignment of the product states may be destroyed, leading to a ''washing out'' of the measured polarization. Among the most important mechanisms that may lead to alignment destruction, are radiation trapping, hyperfine coupling,[16,17] external magnetic fields leading to a Hanle effect depolarization,[16] and depolarization due to secondary collisions.[18,19]

Radiation trapping is negligible because the final state of the observed fluorescence transitions (the $4d$ levels) always have a negligible population. Since more than 93% of the naturally occurring isotope of strontium has no nuclear spin, we can ignore hyperfine depolarization. External magnetic fields at the oven center, due to the heating coils or magnetic bases have been measured and are small in comparison to the earth's magnetic field and can be ignored. Taking the earth's magnetic field value to be ~0.5 G, the Larmor frequency is $\omega_L = (g_J \mu_B B)/\hbar$, where g_J is the Landé factor for the excited final state being considered ($g_J = 1$ for $^1P_1$ and 3/2 for $^3P_2$). This gives a characteristic time scale for depolarization of ~230 ns for the $^1P_1$ level, and ~150 ns for the $^3P_2$ level. The radiative relaxation time τ_r for both levels is ~65 ns and defines the time scale of the measurement. We have estimated the depolarization due to the earth's magnetic field[16] and find that the alignment decreases by only 5% (2%) for the $^3P_2(^1P_1)$ level in the time scale of the measurement. These corrections due to the Hanle effect are small compared to our statistical uncertainties and can be ignored.

The most significant cause for depolarization in our situation is that due to secondary collisions. The alignment decay rate due to secondary collisions $\Gamma_c^{(2)}$ may be related to the perturber density N_p

$$\Gamma_c^{(2)} = N_p \sigma_c^{(2)} \bar{v}, \tag{2}$$

where $\bar{v}$ is the mean relative velocity in the Sr–He collision and $\sigma_c^{(2)}$ is the alignment destroying cross section. This cross section should not depend on the initial laser detuning.

It is most convenient to describe the effect of collisions on the ''longitudinal'' polarization, R, defined by $R = (I_\parallel - I_\perp)/(I_\parallel + 2I_\perp)$, and related to the usual linear polarization by $R = (2P)/(3-P)$. The effects of collisional depolarization on the longitudinal polarization may then be expressed[16,19]

$$\frac{1}{R} = \frac{1}{R_0}\left[\frac{\Gamma_c^{(2)}}{\Gamma_r} + 1\right]. \tag{3}$$

Here, R_0 is the nascent value, $\Gamma_c^{(2)}$ is defined in Eq. (2), and Γ_r is the radiative decay rate. Using Eq. (2) we may rewrite this as

$$\frac{1}{R} = \frac{1}{R_0}\left[\frac{N_p \sigma_c^{(2)} \bar{v}}{\Gamma_r} + 1\right]. \tag{4}$$

Through measurement of $(1/R)$ as a function of the He density we obtain both the nascent longitudinal polarization (R_0) and the collisional depolarization rate coefficients $(\Gamma_c^{(2)}/N_p)$. Experimentally we find,

$$(\Gamma_c^{(2)}/N_p) = (1.3 \pm 0.3) * 10^{-9}\ \ \mathrm{cm}^3/\mathrm{s}$$

for the $6p(^1P_1)$ state, and

$$(\Gamma_c^{(2)}/N_p) = (1.2 \pm 0.5) * 10^{-9}\ \ \mathrm{cm}^3/\mathrm{s}$$

for the $6p(^3P_2)$ state. From these values we see that the time scale for alignment decay is comparable to the radiative lifetime at a perturber pressure of ~2 Torr. Thus we need to make careful measurements of the fluorescence polarization at low pressures. This makes the measurements time consuming since the signal to noise is poor and we have to accumulate enough data points to reduce the error due to counting statistics. Typical runs were over several days for each data point, averaged over 10–20 sets each day. For larger detunings ($\Delta > 50\ \mathrm{cm}^{-1}$), where the signals were very weak, the nascent polarization values were obtained by measuring the polarization at a fixed pressure (~2 Torr) and extrapolating to zero pressure, using the measured alignment decay rates above [see Eq. (4)]. The extrapolated y intercept gives the nascent polarization value for a given detuning. The experimental polarization results are shown in Fig. 2. Error bars include contributions from both the statistical uncertainties at a fixed pressure, and the errors associated with the extrapolation to the zero pressure limit using the measured alignment decay rates.

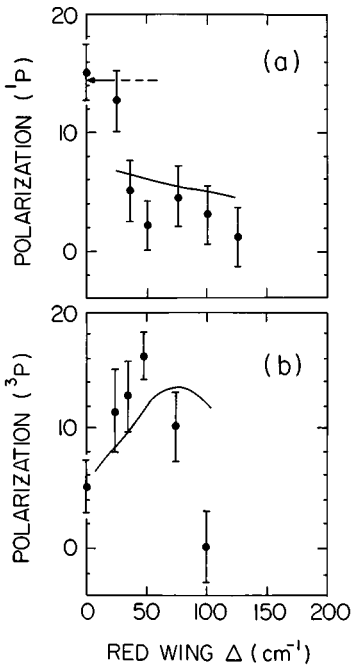

FIG. 2. Linear polarization of collisionally redistributed fluorescence in the (a) quasielastic channel (Sr($6p\ ^1P_1$–$4d\ ^1D_2$)); and (b) spin-changing inelastic channel (Sr($6p\ ^3P_2$–$4d\ ^3D_2$)). Points are experimental values. The solid curves are theoretical model results as described in the text. The arrow gives the expected resonance fluorescence polarization.

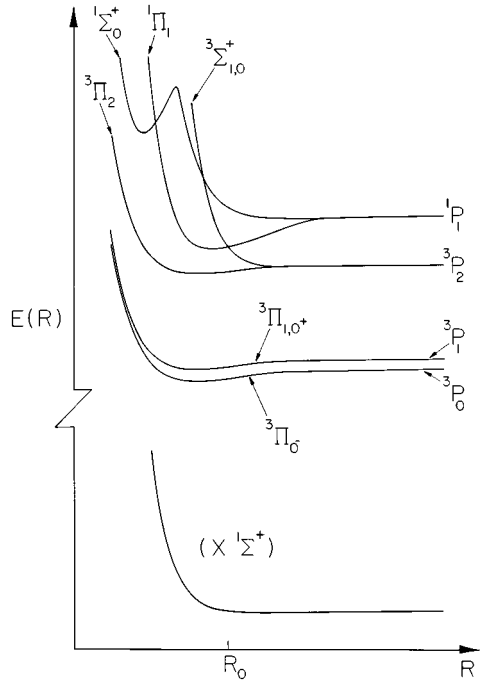

FIG. 3. Sr–He model potential energy curves used in this work. The spin–orbit crossing R_0 is at $\sim 10a_0$.

III. THEORETICAL MODEL

Also shown in Fig. 2, as the solid line, is the result of an analytic calculation based on a Franck–Condon half-collision model, generalizing the orbital-locking and following theory of Lewis and Cooper to this inelastic collision process.[10] This simple model allows great physical insight into the underlying dynamics. In the Lewis–Cooper approach,[10] the radiative excitation is treated as a Franck–Condon transition at a fixed internuclear separation, R_C. This Condon point may be related to the detuning through the quasimolecular difference potential by

$$\hbar\Delta = \hbar(\omega - \omega_0) = V_e(R_C) - V_g(R_C), \tag{5}$$

where V_e and V_g refer to the collisional interaction energies in the excited and ground states, respectively. In the simplest (van der Waals) approximation, R_C is determined by

$$\hbar\Delta = \frac{C_6}{R_C^6}, \tag{6}$$

where C_6 is the difference between the ground and excited state van der Waals constants. In what follows we actually use a set of model potential energy curves. These model potentials are obtained by modifying the MSV (Morse–Spline–van der Waals) potentials of Pouilly[7] for the CaHe molecule. The MSV potentials were adjusted to give reasonable agreement with our previous experimental work on this system including both total absorption profile measurements and the product fine-structure state resolved action spectra.[3] The potential energy curves are shown in Fig. 3. This allows us to correlate excitation at a particular laser frequency in the red wing with internuclear distance in the ($6p\ ^1\Pi$) excited molecular state. For simplicity we neglect any antistatic wing excitation to the repulsive ($6p\ ^1\Sigma^+$) state; this process would not appreciably effect the fluorescence polarization in the $6p\ ^3P_2$ inelastic channel, since there is negligible transfer from the $^1\Sigma^+$ state to the triplet manifold. For the potentials used, the range of detunings (Δ=20–100 cm^{-1}) corresponds to a range of Condon points from $\sim 13a_0$ to $\sim 9a_0$.

The radiative excitation prepares a coherent superposition of $^1\Pi$ molecular states, corresponding to an aligned electronic orbital. This orbital is assumed to follow the rotating internuclear axis adiabatically through the collision, out to a decoupling or locking radius, R_L, beyond which the orbital maintains its space-fixed alignment. The ''proper'' choice of locking radius is a matter of some dispute.[20,21] Rigorously, the locking radius is certainly a function of impact parameter, albeit a slowly varying function.[10–12,20,21] To simplify the presentation here we choose a fixed locking radius of $15a_0$. This choice probably overestimates the actual value, but it simplifies the calculation since now our Condon points will always lie inside R_L. Modifying the theoretical approach for a smaller value of R_L is straightforward, and does not appreciably modify the results or conclusions we present here. The final state alignment can then be predicted analytically in terms of purely geometrical parameters (e.g., the finite rotation angle of electronic orbital through the collision).

Here, we generalize the approach of Lewis and Cooper[10] to the case of redistribution in an inelastic spin-changing collision. The collisional energy transfer process is treated assuming a Landau–Zener transition at a localized spin–orbit $^1\Pi$–$^3\Sigma^+$ curve crossing at R_0. Our choice for the

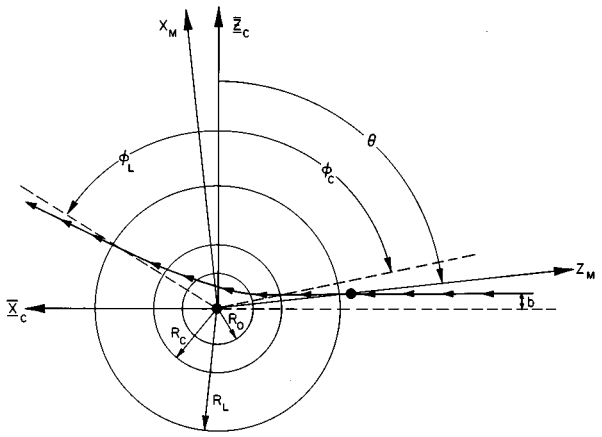

FIG. 4. Scattering diagram allowing space-fixed collision frame and rotating molecule-fixed frame. R_0 is the spin–orbit crossing radius, R_C is the Condon Point of excitation, and R_L is the locking radius.

crossing radius is again determined by our previous studies of the energy transfer process[3] to be $R_0 = 10a_0$.

The discussion can be facilitated by reference to Fig. 4, which shows the space-fixed collision plane, defined such that the collision trajectory lies in the X_cZ_c plane, where the initial relative velocity vector lies along the X_c axis. The collision frame is oriented by a rotation through Euler angles (ξ,χ,ζ) with respect to the laboratory frame (defined by the mutually orthogonal excitation-detection geometry).

We assume, in the far red wing, that radiative excitation occurs to the SrHe($^1\Pi$) state at the Condon point R_C. The excited state wave function may be expanded in a Hund's case (a) basis and has a form which depends on the projection of the laser polarization vector onto the instantaneous molecular transition dipole moment axis

$$|\psi\rangle \propto \sum_{\lambda,\Omega} d^{(1)}_{\lambda\Omega}(\mp\phi_C) D^{*(1)}_{0\lambda}(\xi,\chi,\zeta)[|^1\Pi(\Omega)\rangle]. \tag{7}$$

The summation over Ω is restricted to $\Omega = \pm 1$ for excitation of the Π state in the red wing. As the collision proceeds this excited state wave function evolves through the spin–orbit crossing to

$$|\psi\rangle = \sum_{\lambda,\Omega} d^{(1)}_{\lambda\Omega}(\mp\phi_C) D^{*(1)}_{0\lambda}(\xi,\chi,\zeta) \times [B_\Omega |^1\Pi(\Omega)\rangle + C_\Omega |^3\Sigma^+(\Omega)\rangle], \tag{8}$$

where B_Ω and C_Ω are complex constants which include information about the integrated phase through the collision and interferences associated with the different passages through the Landau–Zener crossing point at R_0. Fortunately, we do not need to know B_Ω and C_Ω in any detail except to note $|B_1| = |B_{-1}|$ and $|C_1| = |C_{-1}|$, since the $\Omega = \pm 1$ states are degenerate (neglecting Λ doubling). The relative phases are determined by the spin–orbit coupling terms[3] and so, $B_1 = B_{-1}$ and $C_1 = -C_{-1}$.

The system then evolves adiabatically to the Hund's case (c) limit

$$|\psi\rangle \overset{t\to\infty}{\to} \sum_{\lambda,\Omega} d^{(1)}_{\lambda\Omega}(\mp\phi_C) D^{*(1)}_{0\lambda}(\xi,\chi,\zeta) \times [B_\Omega |(^1P) j=1,\Omega\rangle + C_\Omega |(^3P) j=2,\Omega\rangle]. \tag{9}$$

We spectrally resolve the fluorescence from the final atomic states, and so they can be treated independently. For the ^1P state we have

$$|\psi\rangle \overset{t\to\infty}{\to} \sum_{\lambda,\Omega} B_\Omega d^{(1)}_{\lambda\Omega}(\mp\phi_C) D^{*(1)}_{0\lambda}(\xi,\chi,\zeta) |j=1,\Omega\rangle. \tag{10}$$

We will not explicate the analysis for the ^1P fluorescence polarization; it is completely analogous to that presented here for the ^3P case, and has previously been given by Lewis *et al.*[10] Our results for the ^1P fluorescence polarization are identical to those in Ref. 10 (for the same choice of classical path and locking radius) and are presented in Fig. 2(a) as the solid line.

For the ^3P channel we experimentally resolve the branching into the fine-structure levels. The dominant branching is to the $^3P_2$ level of interest here. Thus,

$$|\psi\rangle \overset{t\to\infty}{\to} \sum_{\lambda,\Omega} C_\Omega d^{(1)}_{\lambda\Omega}(\mp\phi_C) D^{*(1)}_{0\lambda}(\xi,\chi,\zeta) |j=2,\Omega\rangle. \tag{11}$$

We account for the effect of rotational coupling by a sudden transformation from the molecule fixed to the space-fixed frame at the locking radius R_L. Thus for the ^3P case,

$$|\psi\rangle \propto \sum_{\lambda\Omega\sigma m'} C_\Omega d^{(1)}_{\lambda\Omega}(\mp\phi_C) d^{(2)}_{\Omega\sigma}(-\phi_L) \times D^{(2)}_{m'\sigma}(\xi,\chi,\zeta) D^{*(1)}_{0\lambda}(\xi,\chi,\zeta) |j=2,m'\rangle. \tag{12}$$

The S-matrix element for excitation of a given state $|2,m\rangle$ is given by

$$S_{3_P}(m) \propto \sum_{\lambda\Omega\sigma} C_\Omega d^{(1)}_{\lambda\Omega}(\mp\phi_C) d^{(2)}_{\Omega\sigma}(-\phi_L) \times D^{(2)}_{m\sigma}(\xi,\chi,\zeta) D^{*(1)}_{0\lambda}(\xi,\chi,\zeta). \tag{13}$$

Thus,

$$|S_{3_P}(m)|^2 \propto \sum_{\lambda\lambda'\Omega\Omega'\sigma\sigma'} [C_\Omega C^*_{\Omega'} D^{*(1)}_{0\lambda}(\xi,\chi,\zeta) D^{(1)}_{0\lambda'}(\xi,\chi,\zeta) \times D^{(2)}_{m\sigma}(\xi,\chi,\zeta) D^{*(2)}_{m\sigma'}(\xi,\chi,\zeta) (d^{(1)}_{\lambda\Omega}(\mp\phi_C) \times d^{(1)}_{\lambda'\Omega'}(\mp\phi_C) d^{(2)}_{\Omega\sigma}(-\phi_L) d^{(2)}_{\Omega'\sigma'}(-\phi_L)]. \tag{14}$$

Using angular momentum algebra,[22] this may be simplified to

$$|S_{3_P}(m)|^2$$

$$\propto \sum_{\lambda\lambda'\Omega\Omega'\sigma\sigma'} \sum_{J_3=1,2,3} C_\Omega C_{\Omega'}(2J_3+1)\begin{pmatrix} 1 & 2 & J_3 \\ 0 & m & -m \end{pmatrix} \times \begin{pmatrix} 1 & 2 & J_3 \\ \lambda & \sigma' & -(\lambda+\sigma') \end{pmatrix} D^{(J_3)}_{-m,-(\lambda+\sigma')}(\xi,\chi,\zeta) \times D^{(1)}_{0\lambda'}(\xi,\chi,\zeta) D^{(2)}_{m\sigma}(\xi,\chi,\zeta)(d^{(1)}_{\lambda\Omega}(\mp\phi_C) \times d^{(1)}_{\lambda'\Omega'}(\mp\phi_C) d^{(2)}_{\Omega\sigma}(-\phi_L) d^{(2)}_{\Omega'\sigma'}(-\phi_L)). \tag{15}$$

Averaging over Euler angles yields

$$\langle|S_{3_P}(m)|^2\rangle$$

$$\propto \sum_{\lambda\lambda'\Omega\Omega'\sigma\sigma'} \sum_{J_3} C_\Omega C^*_{\Omega'}(2J_3+1)\begin{pmatrix} 1 & 2 & J_3 \\ 0 & m & -m \end{pmatrix} \times \begin{pmatrix} 1 & 2 & J_3 \\ \lambda & \sigma' & (-\lambda+\sigma') \end{pmatrix} \int d\Omega\ D^{(J_3)}_{-m,-(\lambda+\sigma')}(\xi,\chi,\zeta) \times D^{(1)}_{0\lambda'}(\xi,\chi,\zeta) D^{(2)}_{m\sigma}(\xi,\chi,\zeta) \times (d^{(1)}_{\lambda\Omega}(\mp\phi_C) d^{(1)}_{\lambda'\Omega'} \times (\mp\phi_C) d^{(2)}_{\Omega\sigma}(-\phi_L) d^{(2)}_{\Omega'\sigma'}(-\phi_L)),$$

or

$$\langle|S_{3_P}(m)|^2\rangle$$

$$\propto \sum_{\lambda,\lambda',\Omega,\Omega',\sigma\sigma',J_3} (2J_3+1) C_\Omega C^*_{\Omega'} \begin{pmatrix} 1 & 2 & J_3 \\ 0 & m & -m \end{pmatrix}^2 \times \begin{pmatrix} 1 & 2 & J_3 \\ \lambda & \sigma' & -(\lambda+\sigma') \end{pmatrix} \begin{pmatrix} 1 & 2 & J_3 \\ \lambda' & \sigma & -(\lambda+\sigma') \end{pmatrix} \times [d^{(1)}_{\lambda\Omega}(\mp\phi_C) d^{(1)}_{\lambda'\Omega'}(\mp\phi_C) d^{(2)}_{\Omega\sigma}(-\phi_L) d^{(2)}_{\Omega'\sigma'} \times (-\phi_L)]. \tag{16}$$

This result generalizes the earlier approach of Lewis *et al.*[10] to the inelastic energy transfer channel. Note that the result depends only on the molecular orbital rotation (through ϕ_L and ϕ_C). To evaluate the cross section we need to determine the rotation angles for a given collision trajectory; ϕ_L will also depend, of course, on the choice of locking radius, R_L.

In earlier work by Lewis, Cooper, and co-workers,[10] they found that the choice of a straight line trajectory gave reasonable agreement with the experimental data for the ^1P fluorescence polarization in quasielastic collisional redistribution, at least for small and moderate laser detunings. For small detunings (i.e., large Condon point R_C), the impact parameter weighting in the cross section favors large impact parameter collisions ($b \sim R_C$), and these large impact parameter collisions are well described by a straight line trajectory. However, there was a significant deviation at large detunings (corresponding to small impact parameter collisions); in this limit it was found that a hard sphere collision trajectory gave a better fit to the polarization data.

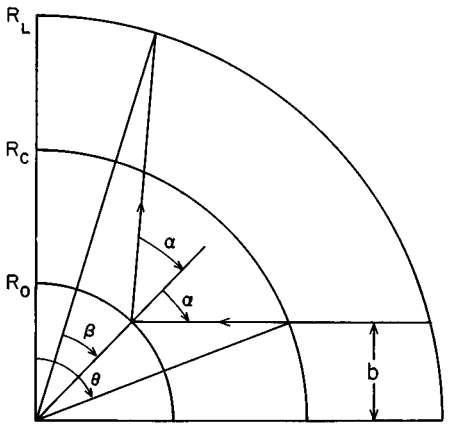

FIG. 5. Hard sphere collision geometry.

In the problem of major interest here, collisional redistribution to the $^3P_2$ channel, the energy transfer proceeds through a short range spin–orbit curve crossing, $R_0 \sim 10a_0$. Thus only small impact parameter collisions will contribute ($b<R_0$). In this case we find that a hard sphere model for the collision trajectory gives significantly better results. This observation is in agreement with our classical path dynamical model which determined scattering angles (for $b<R_0$), close to those predicted by for hard sphere collisions.[2,3] To evaluate the alignment redistribution cross section for the inelastic ^3P channel, we choose the hard sphere radius to be given by the lesser of the values of R_C and R_0.

At first it may appear inconsistent to choose a straight line path to describe the ^1P collisional redistribution, and a hard sphere model to describe the ^3P collisional redistribution, but in fact these choices are dictated by the physics of the process: Quasielastic collisional redistribution to the ^1P state is dominated by larger impact parameter collisions ($b \sim R_C$), and inelastic collisional redistribution to the ^3P manifold is dominated by small impact parameter collisions ($b<R_0$).

Figure 5 shows the collision-geometry for a hard sphere collision. The rotation angles are given by the relations

$$\phi_L = \frac{\pi}{2} - (\alpha+\beta), \tag{17}$$

$$\phi_C = \frac{\pi}{2} - \sin^{-1}\left(\frac{R_0}{R_C}\sin\alpha\right), \tag{18}$$

and

$$\sin\beta = \sin\alpha\left[\sqrt{\left(1-\frac{R_0^2}{R_L^2}\right)+\frac{R_0^2}{R_L^2}\cos^2\alpha}-\frac{R_0}{R_L}\cos\alpha\right] \tag{19}$$

when $R_0<R_C$. When $R_C<R_0$, Eq. (17) becomes

$$\phi_L = \frac{\pi}{2} - \alpha \tag{20}$$

and R_C and R_0 are interchanged in Eqs. (18) and (19).

The impact parameter averages (up to the hard sphere radius) are carried out for each m to obtain the cross sections, $\sigma(j=2,m)$

$$\sigma(j=2,m)\propto 2\pi\int_{\cos^{-1}(R_0/R_C)}^{\pi/2}|\langle S_{3_P}(m)\rangle|^2\cos\theta\, d\theta.$$

The electronic orbital alignment can be related to the collision cross section $\sigma(j,m)$ for populating state $|j,m\rangle$ as

$$A_0^{(2)}(j)=\frac{\Sigma_m[3m^2-j(j+1)]\sigma(j,m)}{j(j+1)\Sigma_m\sigma(j,m)}. \tag{21}$$

The observed linear polarization P may then be related to the alignment by

$$P=\frac{3h^{(2)}(j_i,j_e)A_0^{(2)}(j_i)}{(4+h^{(2)}(j_i,j_e)A_0^{(2)}(j_i))}, \tag{22}$$

where $h^{(2)}(j_i,j_e)$ is an angular momentum dependent factor.[22] For this case $h^{(2)}(j_i=2,j_e=2)=1$. The results from these theoretical calculations are shown in Fig. 2.

IV. RESULTS AND DISCUSSION

The results for the $6p\ ^1P$ fluorescence polarization are shown in Fig. 2(a). The polarization decreases rapidly as the detuning increases away from resonance in the red wing. The resonance fluorescence polarization (at $\Delta=0$) can be easily evaluated[22] as $+14.3\%$. This value is shown by the arrow in Fig. 2(a), and is in good agreement with our experimental result for $\Delta=0$. The observations in Fig. 2(a) are essentially similar to the previous experimental results of Alford *et al.*[9] on the collisional redistribution of polarized light in the first Sr resonance transition [$\mathrm{Sr}(5s^2\ ^1S_0-5s\ 5p\ ^1P_1$]. The theoretical model predictions are also given for a straight line trajectory and are in quite reasonable agreement with the experimental data over the range of detunings investigated here. Again, the theoretical analysis for the quasielastic channel has been given previously by Lewis *et al.*[10] Our model predictions are essentially similar, although for simplicity we have used a slightly different choice of locking radius as discussed above. The theoretical predictions are not particularly sensitive to this choice of locking radius over a range of reasonable values. The experimental results may be understood in terms of the molecular orbital reorientation. As the detuning increases, the range of important impact parameters decreases; as the impact parameter decreases, the total molecular rotation angle through the collision increases leading to a decrease in the residual polarization. For very large detunings (corresponding to very small impact parameters), there will be significant backscattering; in this hard sphere limit the effective molecular orbital rotation is much smaller and the polarization is predicted to increase at very large detunings. We have not reached this limit in our experiment, but Alford *et al.* did observe this type of behavior in their earlier work.[9]

The novel work that we describe here involves our observation of the fluorescence polarization from the inelastic spin change channel ($6p\ ^3P_2$). These results are shown in Fig. 2(b). The observed polarization increases slightly with detuning, to a weak maximum near 50 cm^{-1}, and drops slowly at larger detunings. The theoretical model results, assuming a hard sphere trajectory and a locking radius of $15a_0$, are in fairly good agreement with the experimental data. The model results are insensitive to small changes in the choice for the locking radius, R_L. We have carried out calculations for values of $R_L=11$ and $13a_0$, and find very similar results to those presented in Fig. 2(b). Unfortunately, our experimental data are not sufficiently precise to allow us to place any stringent limit on the locking radius. The observed weak maximum in the theoretical model predictions at ~ 75 cm^{-1} occurs at a detuning where $R_C\sim R_0$, and the assumed hard sphere radius begins to decrease (as R_C). The quantitative agreement between experiment and theory is certainly fortuitous. However, the qualitative agreement indicates a clear understanding of the energy transfer dynamics, and suggests that the orbital-locking and following model may be generalized to a much broader range of collisional processes. This simple analytic approach allows great qualitative insight into the dynamical mechanism.

V. CONCLUSIONS

We have measured the nascent product alignment resulting from the collisional redistribution of polarized light in an inelastic spin-changing energy transfer process. The experimental results are in good agreement with an analytic model based in an orbital-locking and following framework, generalized to this inelastic process. The good agreement indicates a clear understanding of the energy transfer process in this case, and suggests that this simple analytic approach may be generalized to a much broader range of collisional phenomena.

ACKNOWLEDGMENTS

The authors gratefully acknowledge helpful discussions with K. M. Sando and W. C. Stwalley. This work was supported by the National Science Foundation.

[1] K. C. Lin, P. D. Kleiber, J. X. Wang, W. C. Stwalley, and S. R. Leone, J. Chem. Phys. **89**, 4771 (1988); S. Ananthamurthy, P. D. Kleiber, W. C. Stwalley, and K. C. Lin, *ibid.* **90**, 7605 (1989).
[2] S. Ananthamurthy, K. M. Sando, and P. D. Kleiber, J. Chem. Phys. (in press).
[3] S. Ananthamurthy, Ph.D. thesis, University of Iowa, 1993; S. Ananthamurthy, K. M. Sando, and P. D. Kleiber (in preparation).
[4] P. D. Kleiber, in *Chemical Dynamics and Kinetics of Small Radicals*, edited by K. Liu and A. Wagner (World Scientific, New York, in press); and references therein.
[5] M. O. Hale, I. V. Hertel, and S. R. Leone, Phys. Rev. Lett. **53**, 2296 (1984); W. Bussert, D. Neuschäfer, and S. R. Leone, J. Chem. Phys. **87**, 3833 (1987).
[6] P. S. Julienne, Phys. Rev. A **26**, 3299 (1982); P. S. Julienne and F. H. Mies, *ibid.* **30**, 831 (1984).
[7] B. Pouilly, J. Chem. Phys. **95**, 5861 (1991).
[8] L. J. Kovalenko, R. L. Robinson, and S. R. Leone, J. Chem. Soc., Faraday Trans. 2 **85**, 939 (1989).
[9] W. J. Alford, K. Burnett, and J. Cooper, Phys. Rev. A **27**, 1310 (1983); W. J. Alford, N. Andersen, K. Burnett, and J. Cooper, *ibid.* **30**, 2366 (1984).
[10] E. L. Lewis, M. Harris, W. J. Alford, J. Cooper, and K. Burnett, J. Phys. B **16**, 553 (1983); E. L. Lewis, J. M. Salter, and M. Harris, *ibid.* **14**, L173 (1981).
[11] E. E. B. Campbell, H. Schmidt, and I. V. Hertel, Adv. Chem. Phys. **72**, 37 (1988).

[12] J. Grosser, J. Phys. B **14**, 1449 (1981).
[13] M. D. Havey, F. T. Delahanty, L. L. Vahala, and G. E. Copeland, Phys. Rev. A **34**, 2758 (1986); D. A. Olsgaard, M. D. Harvey, and A. Sieradzen, *ibid*. **43**, 6117 (1991).
[14] A. Ermers, T. Woschink, and W. Behmenberg, Z. Phys. D **5**, 113 (1987); W. Behmenberg, Phys. Scr. D **36**, 300 (1987); A. Ermers, W. Behmenberg, and F. Schuller, Z. Phys. D **10**, 437 (1988).
[15] W. J. Alford, Ph.D. thesis, University of Colorado, 1984.
[16] D. Segal and K. Burnett, J. Phys. B **22**, 247 (1989).
[17] I. M. Bell, C. J. K. Quayle, and K. Burnett, Phys. Rev. A **47**, 3128 (1993).
[18] C. G. Carrington and A. Corney, J. Phys. B **4**, 849 (1971).
[19] J. P. Barrat, D. Casalta, J. L. Cojan, and J. Hamel, J. Phys. (Paris) **27**, 608 (1966).
[20] R. J. Bienieck, P. S. Julienne, and F. Rebentrost, J. Phys. B **24**, 5103 (1991).
[21] B. Pouilly and M. H. Alexander, Chem. Phys. **192**, 185 (1992).
[22] R. N. Zare, *Angular Momentum* (Wiley, New York, 1988).